Highly-Robust Organometallic Small-Molecule-based Nonvolatile Resistive Memory Controlled by A Redox-Gated Switching Mechanism

Yang Li,[†,‡,§,⊥] Xiaolin Zhu,[†,⊥] Yujia Li,[†] Mayue Zhang,[†] Chunlan Ma,[†] Hua Li,*[‡] Jianmei Lu,*[‡] and Qichun Zhang*[§]*

[†]Jiangsu Key Laboratory of Micro and Nano Heat Fluid Flow Technology and Energy Application, School of Mathematics and Physics, Suzhou University of Science and Technology, Suzhou, Jiangsu 215009, China

[‡]College of Chemistry, Chemical Engineering and Materials Science, Soochow University, Suzhou 215123, China

[§]School of Materials Science and Engineering, Nanyang Technological University, Singapore 639798, Singapore

KEYWORDS: Nonvolatile memory, redox, organometallic material, data storage, electrical switching

Abstract: Although organic small-molecule-based memory devices (OSMDs) have been demonstrated to show great potential for the application in next-generation data-storage

technology, progress towards their further development has been hugely hindered by the ambiguity of their electrical switching mechanism. Thus, purposely fabricating OSMDs with a definite switching behavior is very urgent. Here, we reported a redox-gated nonvolatile rewritable memory device using an organometallic small molecule as an active material. By introducing the redox-active ferrocene into an organic skeleton, the target small molecule exhibits reliable and robust FLASH-type bistable electrical characteristics with a clear redox-controlled switching mechanism, which leads to low operational voltages, good endurance and long retention. Our study offers a proof-of-concept strategy to design controllable OSMDs with excellent performances.

1. INTRODUCTION

Organic small-molecule-based memory devices (OSMDs) have attracted extensive research interests due to their charming advantages including mechanical flexibility, low-cost fabrication, and ease of processing, as compared to their inorganic counterparts.[1-11] Moreover, some OSMDs succeed to implement multilevel storage in a single device,[12-18] which are considered as the promising candidates for high-density data storage applications. However, despite the above-mentioned appealing advantages, most of the current OSMDs are often faced with the problems of unclear switching behaviors and ambiguous structure–property relationships.[19,20] These material-related problems could input negative effects on the operation of their devices, resulting in energy waste and unsatisfied reproducibility. Therefore, in order to address this issue, designing novel organic small-molecule-based materials with a definite memory switching mechanism is undoubtedly desirable.

Recently, the strategy of incorporating organometallic moieties into polymer structures has emerged as an efficient research progress in organic electronics, such as organic sensors,[21,22] organic batteries,[23,24] and organic light-emitting diodes[25,26]. Compared with single-component polymer material, organometallic polymers can utilize both advantages of the polymers and the incorporated metal center, which can afford unique electronic properties and photoluminescence behavior. In light of this progress, we speculate that introducing a functional redox-active metal into organic small molecular skeleton can effectively overcome the aforementioned problems of OSMDs, leading to high-performance devices. There are two reasons for this consideration: (1) small molecules possess certain structures, which allow for the reliable electron-trapping and -holding for nonvolatile memory applications; and (2) the redox-active metal center can also provide a clear redox-controlled switching mechanism, which could guarantee the successful realization of write–read–erase–read (WRER) cycles and hence invoke highly-robust reprogrammable memory behaviors.

Based on the above-mentioned two points, in this work, we focused on a redox-active moiety, ferrocene, and introduced it into a pyrene-containing conjugated backbone to obtain an organometallic small molecule (**Py-Fc**). The unique 18 π-electrons system of ferrocene has a lot of features, such as solution processability, good thermal stability, and more importantly, satisfactory redox activity.[27] The redox of iron (Fe) center among ferrocene can greatly change its electrical property,[28] thus resulting in different conductivities. Meanwhile, its oxidized form, ferrocenium (Fe^{3+}), can keep stable in the absence of external potential, which provides the possibility of nonvolatility. Therefore, it is logical for us to anticipate that when ferrocene is inserted into a conjugated small molecular backbone, the change of molecular conductivity by redox process would be acquired, which could be utilized as a resistor-type memory.

The proof-of-concept organometallic **Py-Fc** was prepared by combining 1.0 equiv 1-(4-bromophenyl)ferrocene (**2**) and 1.0 equiv 1-ethynylpyrene (**3**) species together through Sonogashira reaction[29] (Scheme 1, see the Supporting Information for details). **Py-Fc** possesses an ethynyl-phenyl spacer as bridge, which links between pyrene and ferrocene unit, enhancing its solubility in many organic solvents including dichlorobenzene, chloroform, and tetrahydrofuran. This target compound was confirmed by NMR (Figure S2 and S3) and elemental analysis. Additionally, **Py-Fc** possesses high decomposing temperature (340 °C is the onset-decomposition temperature with 5% weight-loss, Figure S4). As expected, the as-fabricated metal–organic–metal (MOM) type OSMD of **Py-Fc** exhibits an electrically rewritable switching behavior, with robust WRER operations, high device reproducibility, low write/erase voltages and distinct ON/OFF current ratio, which is a potential contender for nonvolatile data storage applications.

2. RESULTS AND DISCUSSION

2.1. Optical and Electrochemical Properties of Py-Fc. The optical properties of **Py-Fc** were firstly studied in CH_2Cl_2 solution and thin-film state. In solution, **Py-Fc** shows two high-energy absorption peaks at 283 and 305 nm, and two low-energy absorption peaks at 366 and 391 nm, respectively (Figure 1a). The low-energy absorption peaks are attributed to the intra-molecular charge transfer (ICT) process while the high-energy absorption peaks stem from aromatic conjugation.[30] In film state, an apparent bathochromic shift can be clearly seen due to the ICT process. At the same time, the peaks for low-energy absorption shift to 376 and 400 nm with the onset absorption at 443 nm. These shifts of bathochromic absorption are due to molecular aggregation behavior in solid-sate films.

By incorporating ferrocene into the pyrene-based organic backbone, it is supposed that this organometallic small molecule could exhibit enhanced redox behavior. To confirm this, cyclic voltammetry (CV) has been employed to study the electrochemical properties of **Py-Fc**. As shown in Figure 1b, the upper anodic wave represents oxidation process and the bottom cathodic wave stands for reduction pathway. It can be noted that **Py-Fc** shows two kinds of redox peaks rather than one. The reversible couple peaks at 0.43/0.98 V could be assigned to the onset oxidation/reduction potentials of ferrocene center Fe(II), while those at 1.10/–0.25 V correspond to the onset oxidation/reduction potentials of organic pyrene-containing backbone. The reversible redox (reduction of Fe(III) to Fe(II) and oxidation of Fe(II) to Fe(III)) process, arisen from ferrocene under potential, suggests that different molecular charge-storage and -release states could be obtained, which would lead to a resistor-based memory. Moreover, the molecular conjugation of **Py-Fc** allows for efficient charge delocalization, which favors the charge conduction under external electric field.

2.2. Resistive Data Storage Performance of Py-Fc. Taking its redox-active electrochemical properties into consideration, the memory device of **Py-Fc** was obtained by spin-coating its solution onto the ITO-coated substrate, followed by depositing aluminum (Al) as top electrode. The schematic structure of the target two-terminal OSMDs is depicted in Figure 2a. Figure 2b showed the memory behavior of **Py-Fc**-based device, which was examined by sweep-mode current–voltage (*I–V*) characteristics under ambient condition. When electrical potential is carefully applied onto top/bottom electrodes (Al/ITO), **Py-Fc**-based device displays rewritable FLASH-type binary behavior. Under a negative voltage from 0 to −5.0 V, the current presents a sudden increase at −1.6 V (sweep 1), suggesting that this memory device has been set from a LCS (low-conductivity state) to a HCS (high-conductivity state), which corresponds to a “write”

or “SET” stage during data storing process,[31] and the switching voltage is defined as the “SET” voltage (V_{SET}). During the next voltage pulse (sweep 2), the device can maintain its HCS even after the removal of power, which manifests the nonvolatile memory nature. Moreover, its HCS is able to switch back to its initial LCS when we apply a reverse positive bias (sweep 3). This process can be considered as a data “erase” or “RESET” operation. This restored LCS can remain stable under the positive voltage scan (sweep 4), and then this state can be set to HCS again (sweep 5) during the subsequent negative sweep. Such electrically-induced WRER cycle is in good agreement with a binary FLASH memory behavior.

In addition, the LCS and HCS can be clearly detached by more than three orders of magnitude, allowing the memory circuit to clearly distinguish the two-resistance states. Simultaneously, the operational write/erase voltages are small, which are desirable for the sake of low-power-consuming electronics. The cyclic endurance measurement of **Py-Fc**-based memory device was performed in pulse operation mode at a read voltage of 0.1 V. The writing voltage pulse is set to −3.0 V/100 ms, and the erasing voltage pulse is set to +4.0 V/100 ms. The switching time of the device is determined to be about 20 μs. As shown in Figure S5, no evident state fatigue is observed after more than 1.0×10^3 cycles, which indicates satisfactory endurance. The stability of **Py-Fc**-based device was assessed via testing retention time at a continuous read voltage of –1.0 V. The LCS and HCS displays no obvious change for 2.0×10^3 s (Figure 2c). We further investigated the retention tests of the device for a much longer time at a read voltage of –1.0 V and –0.1 V, respectively (Figure S6 and Figure S7). During the tests, there is also no apparent degradation in the resistive states for longer than 1.2×10^4 s, which suggests that the memory device based on **Py-Fc** is endurable under external electrical potential stress. Moreover, in order to examine whether ambient condition (e.g. moisture) affects the device performance, the

memory device was put into an enclosed measurement chamber and tested in nitrogen (N_2) atmosphere instead of ambient condition (Figure S8). Notably, the observed resistive switching characteristic is analogous to that shown in Figure 2b, which manifests good stability under ambient condition. For rewritable OSMDs, switches from one state to another with a different resistance must be reversible, and the states should be stable enough for nonvolatile memory application. From this perspective, it can be concluded that the organometallic redox-active **Py-Fc** is an excellent proof-of-concept contender for FLASH-type data storage.

In order to evaluate the large-sample-size reproducibility of **Py-Fc**, we tested fifty independent units of the devices. The column-chart plot in Figure S9 suggests that the proportion to achieve the bistable memory behaviors of the devices is about 80%, which implies that **Py-Fc** could function as a satisfactory binary FLASH storage media with highly-reliable reproducibility. In addition, an error bar of the statistic distribution of V_{SET} was provided in Figure S9, where V_{SET} locates in the range from –0.8 to –2.6 V. The narrow distribution of V_{SET} also demonstrates the robust cell-to-cell reproducibility of **Py-Fc**-based OSMDs.

2.3. Resistive Switching Mechanism of Py-Fc. Several studies have revealed that the metal electrode could exert an effect on the resistive memory performances (e.g., metal filamentary conduction and intermediate oxide formation).[32-34] To examine whether the Al metal electrode itself and the possibly formed intermediate AlO_x layer influence the OSMD behavior, the top Al electrode was altered into inert gold (Au) and the device with structure of Au/**Py-Fc**/ITO was tested for comparison.[32] As shown in Figure S10, the fabricated device exhibits similar electrical switching behaviors with that using Al as electrode, which indicates that the resistive switching phenomenon is independent of Al and/or AlO_x and belongs to the interior property of the molecule **Py-Fc**. In addition, to confirm the inherent switching characteristics of **Py-Fc**, a thin

layer of 5 nm LiF was inserted between **Py-Fc** and Al metal, which serves as a buffer layer to prevent the contact between the organic film and the electrode.[35,36] The memory device with the structure of Al/LiF/**Py-Fc**/ITO also presents analogous rewritable binary memory performance (Figure S11), which can eliminate the possibility of Al filamentary influence.[35]

The effects of the active layer thickness and electrode area on the resistive switching of **Py-Fc** were further investigated. The devices of Al/**Py-Fc**/ITO with different film thicknesses were obtained by adjusting the concentration of organic solution and systematically compared. The film thickness was determined by the scanning electron microscopy (SEM) images and found to be 60, 80, and 100 nm, respectively. As shown in Figure S12a-S14a, the devices exhibit typical FLASH-type binary memory properties with similar current ratio over 10^3. There is a bit of drift among the SET/RESET operating voltages, which could arise from the morphological variation at different film thickness.[37] Additionally, these devices are observed to be stable with good retention ability (Figure S12b-S14b). Furthermore, the top Al electrode of different sizes was thermally deposited onto the **Py-Fc** film through a shadow mask of circular patterns with different areas of 0.126, 0.0314, and 0.0177 mm^2. All the electrical properties of the devices were characterized under the same condition (Figure S15). It is found that both HCS and LCS are electrode-area dependent. The current value decreases accordingly as the electrode area is reduced, affording the similar current density. It has been reported that the resistive states of memory devices are usually independent of the electrode areas if the metal filaments form in films.[38,39] Therefore, the possibility of resistive switching due to the filamentary conduction could be ruled out.

Recently, it has been shown that the redox processes could be responsible for the resistance switching in some memory devices.[28,40-45] For instance, Valov *et al.*,[40] Tappertzhofen *et al.*,[41] and

Tsuruoka *et al.*[42] have reported the electrochemical redox reactions of ions for resistive switching behaviors. As confirmed by CV results, the underlying switching mechanism of this organometallic **Py-Fc** is closely correlated with the redox activity of ferrocene center, as illustrated in Figure 2d. Such redox process can effectively change the charge density of **Py-Fc** under electric field. As the electric pulse is applied, the gain or loss of the electrons of central Fe atom could alter the charge-storage or -release state of **Py-Fc**, along with the distribution of counter charge cations. Thus, the charge carriers among molecular skeleton would exhibit two distributing states, corresponding to bistable molecular conductivities (LCS and HCS) of **Py-Fc**. In the initial state without electric field, the central Fe atom of ferrocene is in a low valence state (Fe^{2+}), and hence the charge of **Py-Fc** is at a relatively low state, which suggests a low conductivity (LCS). During the SET process, Fe^{2+} ion is oxidized to a higher valence state (Fe^{3+}) by applying negative voltage, and the organic molecule tends to possess more effective counter charge cations. Attributed to this oxidation process, the conductivity of **Py-Fc** becomes higher, leading to HCS. Moreover, in the RESET process, the oxidized Fe^{3+} ion could be reduced to Fe^{2+} again under positive electric stimuli. As a result, the conductivity of **Py-Fc** recovers into the initial LCS and the device is switched off, exhibiting an excellent rewritable FLASH memory behavior. To further verify the redox-controlled switching mechanism of **Py-Fc**, the density functional theory (DFT) was used to calculate the electron distributions of **Py-Fc** (Figure 2e). Based on the data analysis from both the lowest unoccupied molecular orbital (LUMO) and the highest occupied molecular orbital (HOMO), one can easily conclude that the electrons transfer from ferrocene to pyrene side, which matches well with the oxidation process of ferrocene unit ($Fe^{2+} - e^{-} = Fe^{3+}$, see the scheme of charge transfer in Figure S16).

Generally speaking, the device performance directly reflects the intrinsic property of the functional material, that is to say, the performance of the above-mentioned as-fabricated OSMDs can be related to both the solid-state packing mode and the molecular structure of **Py-Fc**: (1) molecular structures determine electronic behaviors while the movement of electrons acts as a key role in controlling the resistive switching mechanism of OSMDs; and (2) molecular packing mode in solid state can greatly affect the efficiency of electron transport, dominating the running parameters of the devices. As discussed above, we have verified that the redox-active property of **Py-Fc** caused by ferrocene is the origin of the rewritable switching behavior. To further get a deeper understanding of the highly reproducible and robust device performance, the studies on PXRD (powder X-ray diffraction) patterns and AFM (atomic force microscope) were conducted as following.

2.4. Organometallic Film Morphology and Nanostructure of Py-Fc. The morphology of **Py-Fc** in film state was examined by AFM (Figure 3). From AFM image (Figure 3a), one can clearly conclude that the as-fabricated film displays a regularly-arranged granular structure (granular size in the range of 100–300 nm), with the root-mean-square roughness (R_{RMS}) of 3.42 nm. This ordered surface morphology could help establishing homogeneous interfaces between the film and top/bottom electrodes, which guarantees the device cell-to-cell reproducibility as observed in the device. Moreover, the 3D-AFM image of **Py-Fc** film shows an interesting multi-hills-like pattern (Figure 3b and 3c) with preferential bottom-up orientation. This uniform molecular growth is able to allow the charges to transfer along the vertical MOM direction, which boosts the formation of desirable charge transporting pathways, and thus lowers operational write/erase voltages of the device.

To further inspect the solid-state nanostructural packing, PXRD measurement of **Py-Fc** film was conducted (Figure 3d). A main diffraction peak (2θ = 9.95°, *d*-spacing = 8.88 Å) in XRD pattern confirms that **Py-Fc** forms a densely-packed lamellar structure in film state.[46,47] Another peak (2θ = 26.6°) is related to the π–π stacking with the distance of 3.35 Å,[48] which suggests that the neighboring conjugated planes of **Py-Fc** have strong interactions. Further DFT calculation affords the optimized molecular geometry of **Py-Fc**, wherein the pyrene and ferrocene locate at each molecular side (Figure 3e, top). The side view visually shows that the pyrene unit is perpendicular to the ferrocene moiety (Figure 3e, bottom). Notably, the height of ferrocene is calculated to be 3.32 Å, which is in good match with π-π interaction distance of 3.35 Å as observed by PXRD. Meanwhile, from the optimized geometry, it can be seen that the pyrene group possesses a good planarity and a high conjugation, which facilitates to induce co-facial stacking. Thus, the π–π stacking peak of PXRD could be ascribed to the intermolecular overlapping of pyrene units. Together with the PXRD-derivated *d*-spacing result, we proposed the reasonable molecular organization manner of **Py-Fc** in film, as illustrated in Figure 3f. The neighboring two **Py-Fc** molecules co-facially overlap with each other over the pyrene plane (conjugated length of 8.88 Å), which is separated by the standing ferrocene with height of 3.35 Å. This oriented co-facial molecular stacking manner controls the film to grow into a homogeneous bottom-up multi-hills-like nanostructure on ITO substrate, which warrants the efficiency of charge conduction in device, and hence leads to a high-performance resistive memory as observed in atmospheric condition.

3. CONCLUSIONS

In summary, we have demonstrated an experimental proof-of-concept nonvolatile organic memory device using a ferrocene-based organometallic small molecule, **Py-Fc**, as an active

storage media. By employing the electric-field-induced electrochemical redox reaction of ferrocene, the **Py-Fc**-based device exhibits excellent rewritable binary memory switching, accompanied with low write/erase voltages, high current ratio and robust reproducibility. Our success in utilizing redox-active material to realize FLASH-type memory opens many possibilities of fabricating multi-redox-gated multilevel OSMDs. Further studies on the strategic design and synthesis of novel multi-redox materials for high-performance multilevel data storage are now under progress.

ASSOCIATED CONTENT

Supporting Information

The Supporting Information is available free of charge on the ACS Publications website. Experimental section, film deposition and device fabrication, ^{1}H and ^{13}C NMR spectra, thermal property, cyclic endurance test, long retention time test, *I*−*V* characteristics of device in N_2 atmosphere, statistical reproducibility and SET voltage distribution of device, *I*−*V* characteristics of Au/**Py-Fc**/ITO, *I*−*V* characteristics of Al/LiF/**Py-Fc**/ITO, *I*−*V* characteristics of device with different film thickness, electrode area dependence of the resistive states, scheme of the charge transfer process, an angle view of the proposed molecular organization, and detailed sweep parameters of the device testing (PDF)

AUTHOR INFORMATION

Corresponding Author

*E-mail: liyang@usts.edu.cn (Y.L.).

*E-mail: lihuaw@suda.edu.cn (H.L.).

*E-mail: lujm@suda.edu.cn (J.L.).

*E-mail: qczhang@ntu.edu.sg (Q.Z.).

Author Contributions

$^{\perp}$Y.L. and X.Z. contributed equally to this work.

Notes

The authors declare no competing financial interest.

ACKNOWLEDGMENT

Q.Z. acknowledges financial support from AcRF Tier 1 (RG 111/17, RG 2/17, RG 114/16, RG 113/18) and Tier 2 (MOE 2017-T2-1-021 and MOE 2018-T2-1-070), Singapore. Y.L. thanks financial support from Natural Science Foundation of Jiangsu Province (BK20190939) and the Natural Science Foundation of the Jiangsu Higher Education Institutions of China (19KJB150018). J.L. and H.L. acknowledges financial support from the National Natural Science Foundation of China (21336005 and 21878199), and the National Excellent Doctoral Dissertation funds of China (201455). This work is also supported by 2019 Undergraduate Innovation and Entrepreneurship Training Program of Jiangsu Province (201910332067Y), the NSF of Jiangsu Higher Education Institutions (17KJA140001), Six Talent Peaks Project of Jiangsu Province, China (XCL-078), and Jiangsu Key Disciplines of the Thirteenth Five-Year Plan (20168765).

REFERENCES

(1) Gao, S.; Yi, X.; Shang, J.; Liu, G.; Li, R.-W., Organic and Hybrid Resistive Switching Materials and Devices. *Chem. Soc. Rev.* **2019**, *48*, 1531-1565.

(2) Busche, C.; Vilà-Nadal, L.; Yan, J.; Miras, H. N.; Long, D.-L.; Georgiev, V. P.; Asenov, A.; Pedersen, R. H.; Gadegaard, N.; Mirza, M. M.; Paul, D. J.; Poblet, J. M.; Cronin, L., Design and Fabrication of Memory Devices Based on Nanoscale Polyoxometalate Clusters. *Nature* **2014**, *515*, 545-549.

(3) Li, W.; Guo, F.; Ling, H.; Liu, H.; Yi, M.; Zhang, P.; Wang, W.; Xie, L.; Huang, W., Solution-Processed Wide-Bandgap Organic Semiconductor Nanostructures Arrays for Nonvolatile Organic Field-Effect Transistor Memory. *Small* **2018**, *14*, 1701437.

(4) Cha, A. N.; Lee, S. A.; Bae, S.; Lee, S. H.; Lee, D. S.; Wang, G.; Kim, T. W., An All-Organic Composite System for Resistive Change Memory via the Self-Assembly of Plastic-Crystalline Molecules. *ACS Appl. Mater. Interfaces* **2017**, *9*, 2730-2738.

(5) Yang, F.; Zhao, Q.; Xu, C.; Zou, Y.; Dong, H.; Zheng, Y.; Hu, W., Unveiling the Switching Riddle of Silver Tetracyanoquinodimethane Towards Novel Planar Single-Crystalline Electrochemical Metallization Memories. *Adv. Mater.* **2016**, *28*, 7094-7100.

(6) Gu, P.; Gao, J.; Lu, C.-J.; Wang, C.; Li, G.; Zhou, F.; Xu, Q.-F.; Lu, J.-M.; Zhang, Q., Synthesis of Tetranitro-oxacalix[4]arene with Oligoheteroacene Groups and Its Nonvolatile Ternary Memory Performance. *Mater. Horiz.*, **2014**, *1*, 446-451.

(7) Poon, C. T.; Wu, D.; Yam, V. W., Boron(III)-Containing Donor-Acceptor Compound with Goldlike Reflective Behavior for Organic Resistive Memory Devices. *Angew. Chem. Int. Ed.* **2016**, *55*, 3647-3651.

(8) Chen, H.; Cheng, N.; Ma, W.; Li, M.; Hu, S.; Gu, L.; Meng, S.; Guo, X., Design of a Photoactive Hybrid Bilayer Dielectric for Flexible Nonvolatile Organic Memory Transistors. *ACS nano* **2016**, *10*, 436-445.

(9) Wu, Z.-H.; Sun, W.-J.; Tian, H.-H.; Yu, Z.-F.; Guo, R.-X.; Shao, X.; Zhang, H.-L., 9,10-

Imide-Pyrene-Fused Pyrazaacenes (IPPA) as N-Type Doping Materials for High-Performance Nonvolatile Organic Field Effect Transistor Memory Devices. *Adv. Electron. Mater.* **2019**, *5*, 1800598.

(10) Li, G.; Zheng, K.; Wang, C.; Leck, K. S.; Hu, F.; Sun, X. W.; Zhang, Q., Synthesis and Nonvolatile Memory Behaviors of Dioxatetraazapentacene Derivatives. *ACS Appl. Mater. Interface*, **2013**, *5*, 6458–6462.

(11) Lee, W.-Y.; Kurosawa, T.; Lin, S.-T.; Higashihara, T.; Ueda, M.; Chen, W.-C., New Donor–Acceptor Oligoimides for High-Performance Nonvolatile Memory Devices. *Chem. Mater.* **2011**, *23*, 4487-4497.

(12) Chan, H.; Wong, H.-L.; Ng, M.; Poon, C.-T.; Yam, V. W.-W., Switching of Resistive Memory Behavior from Binary to Ternary Logic via Alteration of Substituent Positioning on the Subphthalocyanine Core. *J. Am. Chem. Soc.* **2017**, *139*, 7256-7263.

(13) Liu, Z.; He, J.; Li, H.; Xu, Q.; Li, N.; Chen, D.; Wang, L.; Chen, X.; Zhang, K.; Lu, J., Organic Multilevel Memory Devices of Long-Term Environmental Stability via Incorporation of Fluorine. *Adv. Electron. Mater.* **2016**, *2*, 1500474.

(14) Leydecker, T.; Herder, M.; Pavlica, E.; Bratina, G.; Hecht, S.; Orgiu, E.; Samorì, P., Flexible Non-Volatile Optical Memory Thin-Film Transistor Device with Over 256 Distinct Levels Based on an Organic Bicomponent Blend. *Nature Nanotechnol.* **2016**, *11*, 769-775.

(15) Hong, E. Y.; Poon, C. T.; Yam, V. W., A Phosphole Oxide-Containing Organogold(III) Complex for Solution-Processable Resistive Memory Devices with Ternary Memory Performances. *J. Am. Chem. Soc.* **2016**, *138*, 6368-6371.

(16) Li, Y.; Zhang, C.; Gu, P.; Wang, Z.; Li, Z.; Li, H.; Lu, J.; Zhang, Q., Nonvolatile Tri-State Resistive Memory Behavior of a Stable Pyrene-Fused N-Heteroacene with Ten Linearly-

Annulated Rings. *Chem. Eur. J.* **2018**, *24*, 7845-7851.

(17) Wang, C.; Gu, P.; Hu, B.; Zhang, Q., Recent Progress in Organic Resistance Memory with Small Molecules and Inorganic–Organic Hybrid Polymers as Active Elements. *J. Mater. Chem. C* **2015**, *3*, 10055-10065.

(18) Cui, B. B.; Tang, J. H.; Yao, J.; Zhong, Y. W., A Molecular Platform for Multistate Near-Infrared Electrochromism and Flip-Flop, Flip-Flap-Flop, and Ternary Memory. *Angew. Chem. Int. Ed.* **2015**, *54*, 9192-9197.

(19) Song, Y.; Lee, T., Electronic Noise Analyses on Organic Electronic Devices. *J. Mater. Chem. C* **2017**, *5*, 7123-7141.

(20) Qian, Y.; Zhang, X.; Xie, L.; Qi, D.; Chandran, B. K.; Chen, X.; Huang, W., Stretchable Organic Semiconductor Devices. *Adv. Mater.* **2016**, *28*, 9243-9265.

(21) Maldonado, N.; Vegas, V. G.; Halevi, O.; Martínez, J. I.; Lee, P. S.; Magdassi, S.; Wharmby, M. T.; Platero-Prats, A. E.; Moreno, C.; Zamora, F.; Amo-Ochoa, P., 3D Printing of a Thermo- and Solvatochromic Composite Material Based on a Cu(II)–Thymine Coordination Polymer with Moisture Sensing Capabilities. *Adv. Funct. Mater.* **2019**, *29*, 1808424.

(22) Guan, W.; Zhou, W.; Lu, J.; Lu, C., Luminescent Films for Chemo- and Biosensing. *Chem. Soc. Rev.* **2015**, *44*, 6981-7009.

(23) Xiang, J.; Burges, R.; Häupler, B.; Wild, A.; Schubert, U. S.; Ho, C.-L.; Wong, W.-Y., Synthesis, Characterization and Charge–Discharge Studies of Ferrocene-Containing Poly(fluorenylethynylene) Derivatives as Organic Cathode Materials. *Polymer* **2015**, *68*, 328-334.

(24) Zhong, H.; Wang, G.; Song, Z.; Li, X.; Tang, H.; Zhou, Y.; Zhan, H., Organometallic Polymer Material for Energy Storage. *Chem Commun.* **2014**, *50*, 6768-6770.

(25) Bao, R.; Wang, C.; Dong, L.; Yu, R.; Zhao, K.; Wang, Z. L.; Pan, C., Flexible and Controllable Piezo-Phototronic Pressure Mapping Sensor Matrix by ZnO NW/p-Polymer LED Array. *Adv. Funct. Mater.* **2015**, *25*, 2884-2891.

(26) Happ, B.; Winter, A.; Hager, M. D.; Schubert, U. S., Photogenerated Avenues in Macromolecules Containing Re(I), Ru(II), Os(II), and Ir(III) Metal Complexes of Pyridine-Based Ligands. *Chem. Soc. Rev.* **2012**, *41*, 2222-2255.

(27) Astruc, D., Why is Ferrocene so Exceptional? *Eur. J. Inorg. Chem.* **2017**, *2017*, 6-29.

(28) Shao, J.-Y.; Cui, B.-B.; Tang, J.-H.; Zhong, Y.-W., Resistive Memory Switching of Transition-Metal Complexes Controlled by Ligand Design. *Coord. Chem. Rev.* **2019**, *393*, 21-36.

(29) He, B.; Pun, A. B.; Klivansky, L. M.; McGough, A. M.; Ye, Y.; Zhu, J.; Guo, J.; Teat, S. J.; Liu, Y., Thiophene Fused Azacoronenes: Regioselective Synthesis, Self-Organization, Charge Transport and Its Incorporation in Conjugated Polymers. *Chem. Mater.* **2014**, *26*, 3920-3927.

(30) Dhokale, B.; Jadhav, T.; Mobin, S. M.; Misra, R., Synergistic Effect of Donors on Tetracyanobutadine (TCBD) Substituted Ferrocenyl Pyrenes. *RSC Adv.* **2015**, *5*, 57692-57699.

(31) Hu, B.; Wang, C.; Wang, J.; Gao, J.; Wang, K.; Wu, J.; Zhang, G.; Cheng, W.; Venkateswarlu, B.; Wang, M.; Lee, P. S.; Zhang, Q., Inorganic–Organic Hybrid Polymer with Multiple Redox for High-Density Data Storage. *Chem. Sci.* **2014**, *5*, 3404-3408.

(32) Cho, D.-Y.; Luebben, M.; Wiefels, S.; Lee, K.-S.; Valov, I. Interfacial Metal−Oxide Interactions in Resistive Switching Memories. *ACS Appl. Mater. Interfaces* **2017**, *9*, 19287-19295.

(33) Wedig, A.; Luebben, M.; Cho, D.-Y.; Moors, M.; Skaja, K.; Rana, V.; Hasegawa, T.; Adepalli, K. K.; Yildiz, B.; Waser, R.; Valov, I. Nanoscale Cation Motion in TaO_x, HfO_x and TiO_x Memristive Systems. *Nat. Nanotechnol.* **2016**, *11*, 67-74.

(34) Ling, H.; Yi, M.; Nagai, M.; Xie, L.; Wang, L.; Hu, B.; Huang, W., Controllable Organic Resistive Switching Achieved by One-Step Integration of Cone-Shaped Contact. *Adv. Mater.* **2017**, *29*, 1701333.

(35) Zhang, Q.; He, J.; Zhuang, H.; Li, H.; Li, N.; Xu, Q.; Chen, D.; Lu, J. Rational Design of Small Molecules to Implement Organic Quaternary Memory Devices. *Adv. Funct. Mater.* **2016**, *26*, 146-154.

(36) Liu, Z.; Shi, E.; Wan, Y.; Li, N.; Chen, D.; Xu, Q.; Li, H.; Lu, J.; Zhang, K.; Wang, L., Effects of Gradual Oxidation of Aromatic Sulphur-Heterocycle Derivatives on Multilevel Memory Data Storage Performance. *J. Mater. Chem. C* **2015**, *3*, 2033-2039.

(37) Li, L.; Gao, P.; Wang, W.; Mullen, K.; Fuchs, H.; Chi, L. Growth of Ultrathin Organic Semiconductor Microstripes with Thickness Control in the Monolayer Precision. *Angew. Chem. Int. Ed.* **2013**, *52*, 12530-12535.

(38) Yang, C.-S.; Shang, D.-S.; Chai, Y.-S.; Yan, L.-Q.; Shen, B.-G.; Sun, Y. Moisture Effects on the Electrochemical Reaction and Resistance Switching at Ag/Molybdenum Oxide Interfaces. *Phys. Chem. Chem. Phys.* **2016**, *18*, 12466-12475.

(39) Lim, S. L.; Li, N. J.; Lu, J. M.; Ling, Q. D.; Zhu, C. X.; Kang, E. T.; Neoh, K. G., Conductivity Switching and Electronic Memory Effect in Polymers with Pendant Azobenzene Chromophores. *ACS Appl. Mater. Interfaces* **2009**, *1*, 60-71.

(40) Valov, I. Redox-Based Resistive Switching Memories (ReRAMs): Electrochemical Systems at the Atomic Scale. *Chem. Electro. Chem.* **2014**, *1*, 26-36.

(41) Tappertzhofen, S.; Menzel, S.; Valov, I.; Waser, R. Redox Processes in Silicon Dioxide Thin Films Using Copper Microelectrodes. *Appl. Phys. Lett.* **2011**, *99*, 203103.

(42) Tsuruoka, T.; Valov, I.; Tappertzhofen, S.; Hurk, J.; Hasegawa, T.; Waser, R.; Aono, M.

Redox Reactions at Cu,Ag/Ta_2O_5 Interfaces and the Effects of $Ta2O_5$ Film Density on the Forming Process in Atomic Switch Structures. *Adv. Funct. Mater.* **2015**, *25*, 6374-6381.

(43) Hasegawa, T.; Terabe, K.; Tsuruoka, T.; Aono, M. Atomic Switch: Atom/Ion Movement Controlled Devices for Beyond Von-Neumann Computers. *Adv. Mater.* **2012**, *24*, 252-267.

(44) Tappertzhofen, S.; Valov, I.; Tsuruoka, T.; Hasegawa, T.; Waser, R.; Aono, M. Generic Relevance of Counter Charges for Cation-Based Nanoscale Resistive Switching Memories. *ACS Nano* **2013**, *7*, 6396-6402.

(45) Yang, Y.; Gao, P.; Li, L.; Pan, X.; Tappertzhofen, S.; Choi, S.; Waser, R.; Valov, I.; Lu, W. D. Electrochemical Dynamics of Nanoscale Metallic Inclusions in Dielectrics. *Nat. Commun.* **2014**, *5*, 4232.

(46) Yun, H. J.; Lee, G. B.; Chung, D. S.; Kim, Y. H.; Kwon, S. K., Novel Diketopyrroloppyrrole Random Copolymers: High Charge-Carrier Mobility from Environmentally Benign Processing. *Adv. Mater.* **2014**, *26*, 6612-6616.

(47) Kim, Y.; Cook, S.; Tuladhar, S. M.; Choulis, S. A.; Nelson, J.; Durrant, J. R.; Bradley, D. D. C.; Giles, M.; McCulloch, I.; Ha, C.-S.; Ree, M., A Strong Regioregularity Effect in Self-Organizing Conjugated Polymer Films and High-Efficiency Polythiophene: Fullerene Solar Cells. *Nature Mater.* **2006**, *5*, 197-203.

(48) Yi, Z.; Ma, L.; Chen, B.; Chen, D.; Chen, X.; Qin, J.; Zhan, X.; Liu, Y.; Ong, W. J.; Li, J., Effect of the Longer β-Unsubstituted Oliogothiophene Unit (6T and 7T) on the Organic Thin-Film Transistor Performances of Diketopyrrolopyrrole-Oliogothiophene Copolymers. *Chem. Mater.* **2013**, *25*, 4290-4296.

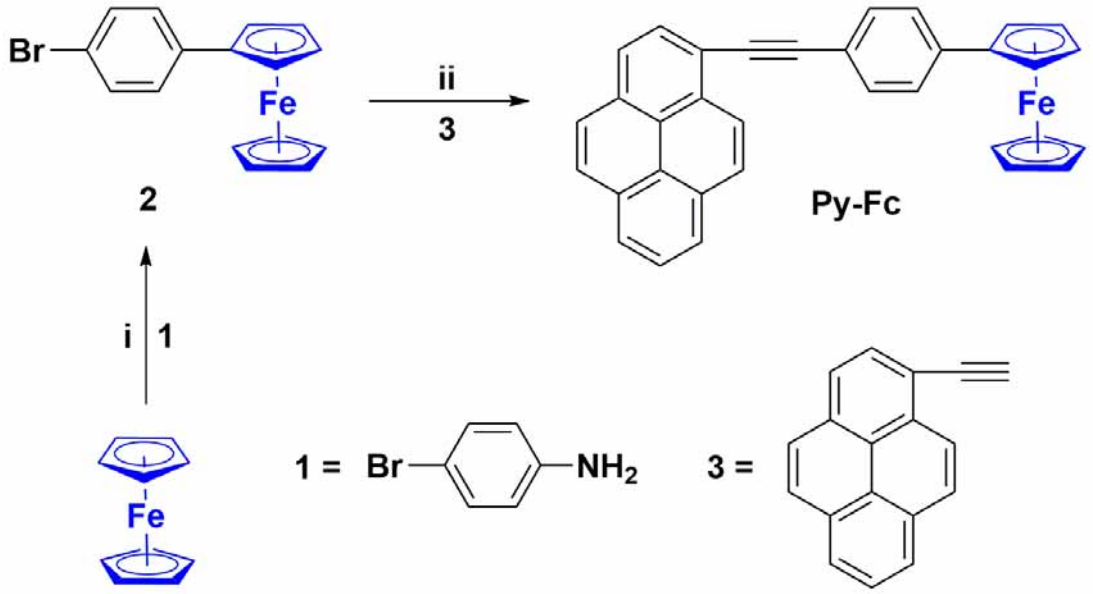

Scheme 1. Synthesis of the redox-active organometallic **Py-Fc**. (i) $H_2SO_4/H_2O/NaNO_2$, 64%; (ii) $CuI/Pd(PPh_3)_2Cl_2/Et_3N/THF$, 40%.

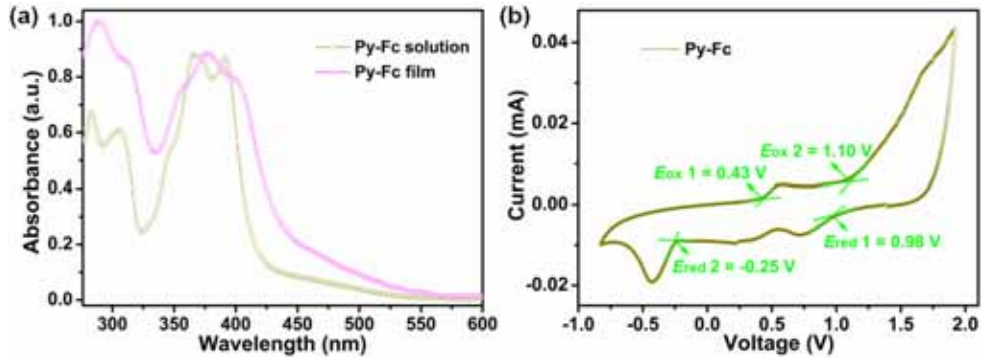

Figure 1. (a) UV-Vis spectra of **Py-Fc** in CH_2Cl_2 (ca. 1.0×10^{-4} mol/L) and thin film. (b) Cyclic voltammogram curve of **Py-Fc** at a scan rate of 50 mV s^{-1}.

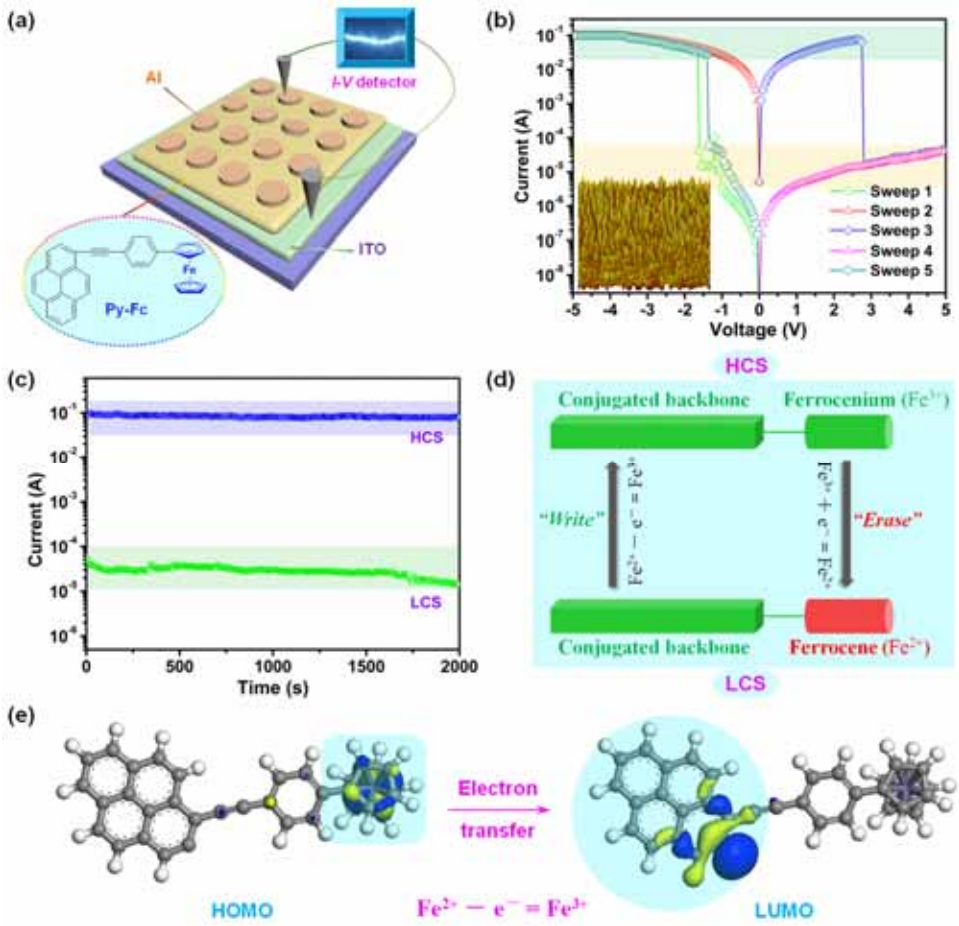

Figure 2. (a) Scheme of the MOM-type OSMD structure. (b) The detected *I–V* characterization of OSMDs and the inset denotes the surface morphology of **Py-Fc** active layer. (c) Retention stability of **Py-Fc**-based OSMDs at LCS and HCS at a "read" potential of –1.0 V. (d) Redox-controlled write/erase mechanism for memory behavior of **Py-Fc**. (e) DFT calculated HOMO and LUMO molecular iso-surfaces of **Py-Fc**.

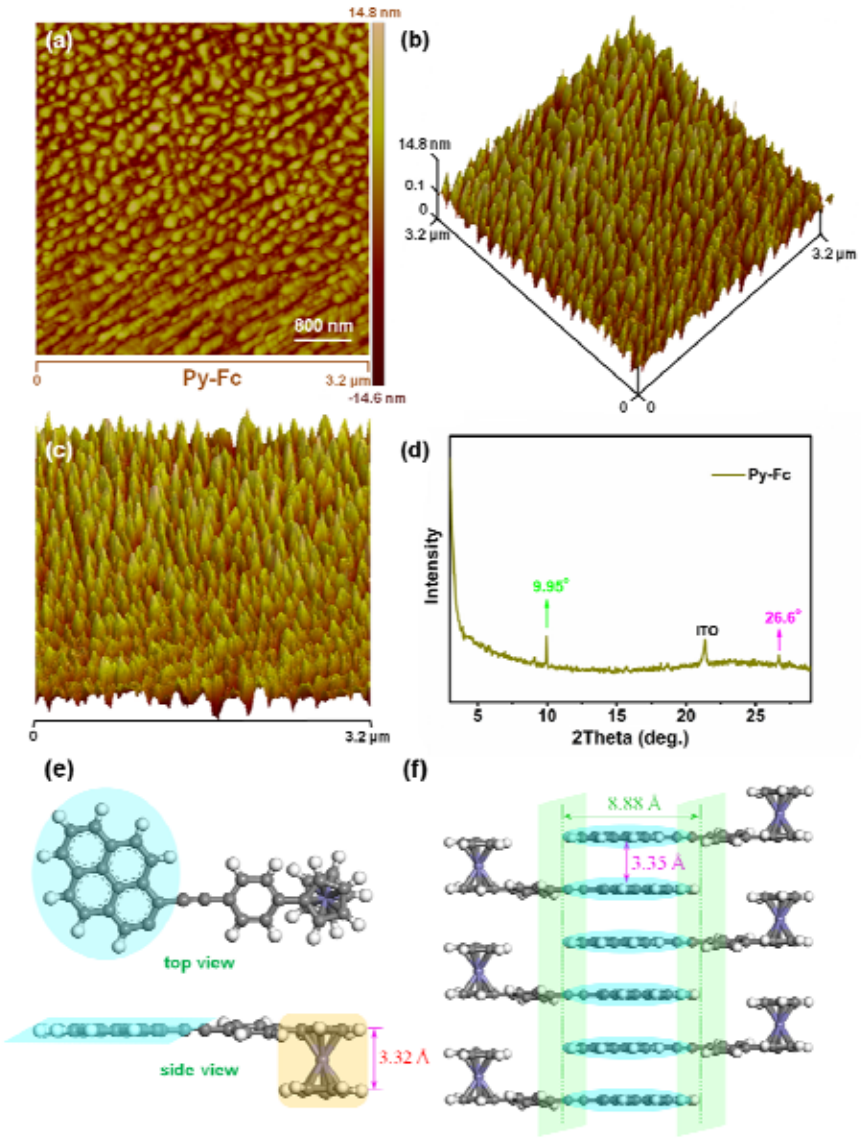

Figure 3. (a) AFM image of **Py-Fc**-based film as spun onto ITO substrate. The scale bar is 800 nm. (b, c) 3D-AFM pictures of **Py-Fc**-based film: (b) an angle view; (c) top view. (d) PXRD pattern of **Py-Fc**-based film as spun onto ITO substrate. The peak located at 2θ = 20.3° represents the intrinsic reflection from ITO. (e) Top view and side view of optimized molecular condiguration of **Py-Fc** through DFT calculation. The gray, white and light-purple spheres represent carbon, hydrogen and iron atom, respectively. (f) Illustration of the proposed molecular organization of **Py-Fc** in film state on ITO substrate.

TOC:

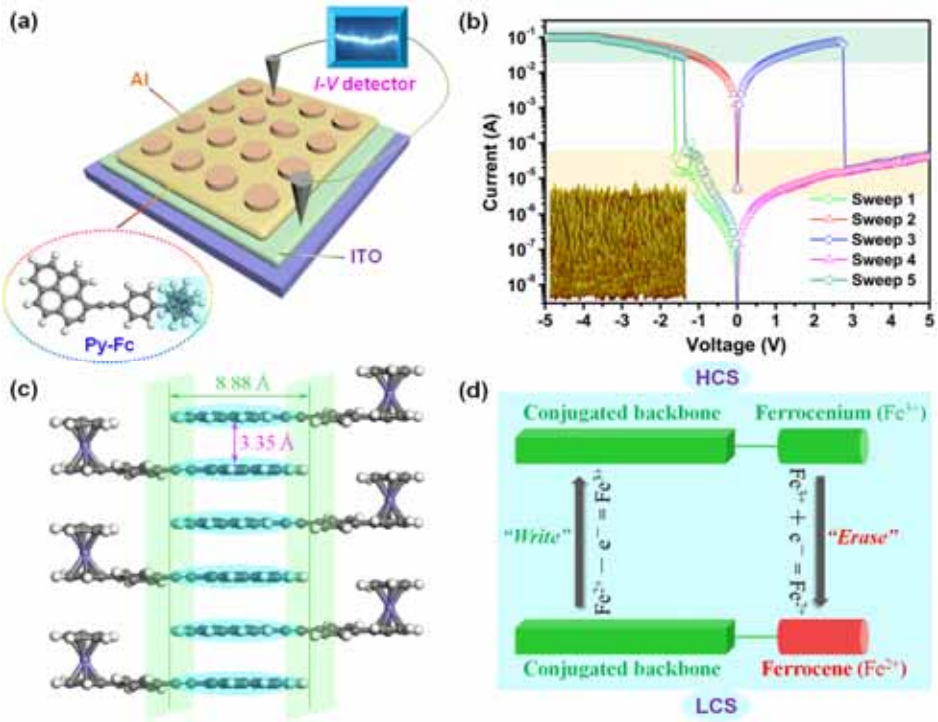
(a)
Al
I-V detector
ITO
Py-Fc
(b)
Current (A)
Voltage (V)
Sweep 1
Sweep 2
Sweep 3
Sweep 4
Sweep 5
HCS
(c)
8.88 Å
3.35 Å
(d)
Conjugated backbone
Ferrocenium (Fe3+)
"Write"
Fe2+ − e− = Fe3+
Fe3+ + e− = Fe2+
"Erase"
Conjugated backbone
Ferrocene (Fe2+)
LCS